Thermo-Hydraulic Performance Analysis of Hybrid Enhanced Microchannel Heat Sink Designs

Taha Boussaid
CETHIL, UMR 5008
INSA Lyon, CNRS
taha.boussaid@insa-lyon.fr

Kamyar Motaghedolhagh
Dept of Mech Eng
University College London
k.motaghedolhagh@ucl.ac.uk

Azadeh Shariati
Dept of Mech Eng
University College London
a.shariati@ucl.ac.uk

Mehdi Baghdadi
Dept of Mech Eng
University College London
m.baghdadi@ucl.ac.uk

***Abstract*—Heat sinks using microchannels can efficiently extract dense heat fluxes from high-power electronic devices at relatively low chip temperatures. The current challenges remain in minimising the thermal gradient on the heated wall and gaining a better understanding of the two-phase heat transfer mechanisms. It is within this scope that new straight geometric configurations are proposed in this paper to reduce the thermal gradient on the backside of the MCHS. Moreover, an investigation of the nanofluid concentration on the hydrothermal performance is explored. For each design, a performance analysis has been conducted on the geometrical and physical parameters involved in dissipating a heat flux of q = 100W/cm^2. The final outcome is a hybrid design consisting of ribs and subdivided microchannels with an average heated wall temperature of 41°C under a total pressure drop of 18.57 kPa.**

***Index Terms*—Heat sink design, Microchannel, Thermo-hydraulic performance, CFD**

I. Introduction

The current energy transition leads to a preference for electric energy over other energy vectors such as gas and fossil fuels. Thus, the transport market is undergoing a metamorphosis towards a 100% electric car fleet. Electric cars include a variety of power transducers, often a group of inverters, choppers, and rectifiers as part of their drive-train. Due to the operating frequencies, converter elements are the site of significant heat generation, which induces a temperature rise in the chips. Regarding the thermal resistance of the materials used for the manufacture of these chips, the operating temperature should ideally not exceed 360K, but still, the maximum allowed temperature is around 398K. Above this temperature, efficiency losses become very high, and the microchips may be completely damaged [1]. Moreover, the current generation of dense microchip packages that function at high frequencies—resulting in a very high heat flux on electronic devices—has made thermal management of power electronic devices an important research topic in the last few years. Although a well-designed fin heat sink using air as a coolant is the simplest cooling technique, it has low cooling efficiency, and the fan itself produces heat. Air-based pin-fin cooling schemes cannot be used for dissipating heat in excess of $60W/cm^2$ while maintaining the device at proper operating temperatures [2]. Faced with this insufficient heat transfer with air as a coolant, mainly due to the thermophysical properties of air, there has been a shift towards other modes of heat transfer, such as forced convection with liquids. One of the techniques that has attracted the attention of researchers is microchannel cooling technology. Since the prototype of a microchannel heat sink (MCHS) [3], where the heat transfer rate was $q = 790W/cm^2$ for a total pressure drop penalty of $\Delta p = 200kPa$, the scientific research community covering the fields of fluid dynamics, heat transfers, and thermofluids showed a great interest in this cooling system. Several improvement methodologies have been explored and implemented, all with the same goal of intensifying heat transfer while minimising the pressure drop and temperature gradient. These improvement methodologies are usually classified into two categories, as in [4]: active methods, where heat transfer is improved by using external energy like vibrations or electric and magnetic fields, and passive methods where the improvement of heat transfer relies on geometrical modifications, heat transfer mechanisms, and fluid additives. Although less interest was given to active methods, due mainly to the complexity of implementing such methods. Two categories can be distinguished. The first category consists of techniques that directly affect the fluid (thermal conductivity k, permittivity ε, ...) by using nanofluids and external magnetic field [5]. The second one involves acting on the fluid by deforming a solid wall [6]. In passive methods, when the enhancement method is purely geometrical, ribs and pin-fins are generally introduced in the design. For example, an interrupted microchannel design with double circular pin-fins (Fig. 1), was investigated. The numerical results showed that introducing pin-fins provides excellent heat transfer enhancement and better wall temperature uniformity. This improvement is due to the disruption of the thermal boundary layer in each zone of the pin-fins, as well as the induced fluid mixing. However, the pressure drop was significantly sensitive to the pin-fin diameter, and an optimum has to be found for each configuration [7]. Similar analyses of different fin shapes and arrangements were conducted in [8]. In [9], a genetic algorithm was used to optimize a Y-shaped fractal network microchannel design. A multi-objective constraint was simultaneously applied to the model aiming to decrease the total thermal resistance and the pressure drop by varying geometrical quantities. The optimized design showed a maximum heated wall temperature of $T_{\max} = 347.5K$ for a $q = 100W/cm^2$ heat flux, and the required pump power was $\dot{W}_{\text{pump}} = 32.5mW$.

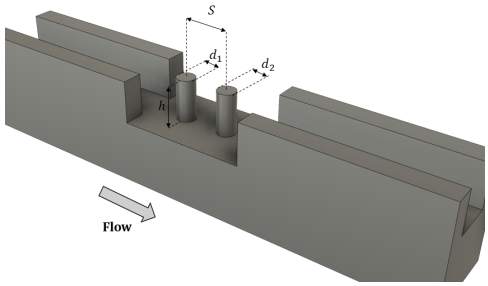

Fig. 1: Schematic diagram of an interrupted single microchannel with two cylindrical fin-pins studied in [7].

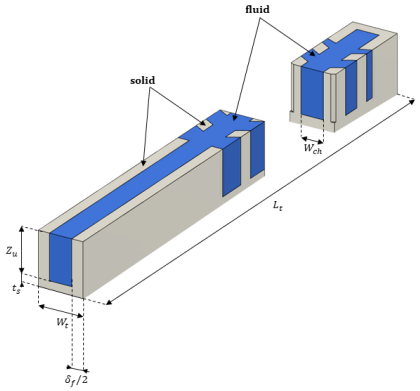

Fig. 2: Common geometrical quantities for the studied designs. L_t is total length of the MCHS, W_t the total width of the unit cell, W_{ch} the wetted microchannel width, Z_u the microchannel depth, δ_f the fin thickness and t_s the solid wall thickness.

Another improvement option that has been widely explored is boiling flows in microchannels [10]. This method benefits from a better heat transfer rate as latent heat of vaporisation is involved, in addition to sensible heat. The current trend is focusing on combining these different passive methods, which is referred to as hybrid methods [11]. Recent studies mainly explored the use of additives such as *nanofluids* to enhance heat transfer by increasing the thermal conductivity of the coolant [4]. All studies in [12], [13] agree that MCHS cooling performances are well enhanced when the particle volume fraction, ϕ, is increased and the nanoparticle size is decreased. Conversely, this thermal enhancement is accompanied by a higher pressure drop due to nanoparticle deposition, Brownian motion, and the resulting higher dynamic viscosity [12].

The most commonly used nanoparticle materials are Aluminium Oxide (Al_2O_3), Zinc Oxide (ZnO), Copper Oxide (CuO), and Silicone Dioxide (SiO_2). Hybrid nanofluids were also studied in [12] by combining different nanoparticles for a given coolant. However, one of the current problems with using nanofluids is essentially related to fouling resistance, which increases with time, resulting in more nanoparticles being deposited on the surface of the microchannel. One suggested solution would be investigating curved MCHS designs, as curved flows generate secondary flows and a self-cleaning effect, as found in spiral heat exchangers.

II. Description of the Proposed Designs

In this paper, we conduct an in-depth numerical performance analysis. The heat sink's total length is fixed at $L_t = 10mm$, with a unit cell width of $L_{unit} = 500\mu m$. The microchannel and fins widths are both $W_{ch} = \delta_f = 250\mu m$. The fluid region and the dimensions of the inlet and outlet are consistent across all four designs, with fixed cross-sectional dimensions of $200 \times 250\mu m^2$, as illustrated in Fig. 2. The schematic diagram of the studied designs is depicted in Fig. 3. In the following, OFM represents Oblique Fins Microchannel, SCM denotes Smooth Conventional Microchannel, RRM signifies Rectangular Ribs Microchannel, RROFM indicates Rectangular Ribs Oblique Fins Microchannel, and RRSDM stands for Rectangular Ribs and Subdivided Microchannel.

The aim of oblique fins is to reduce the flow length and enhance heat transfer at the end by disrupting the thermal boundary layer. However, the downside of these structures is that they induce fluid stagnation on their backs, which explains their introduction only in the second part of the microchannel. Their dimensions (L_f, β) will be varied in the present work in order to investigate the resulting effects, as shown in Fig. 4. Designs RRM, RROFM, and RRSDM include the insertion of ribs which aim to disrupt the thermal boundary layer. As for the oblique fins, their thermal and hydraulic effects will be investigated by varying their geometric parameters (L_r, e_r, N_r) as presented in Fig. 5. Uniform heat flux is applied at the base solid wall which is made of Copper for steady state simulations and the other solid walls are assumed to be adiabatic due to symmetry. Finally, water and Al_2O_3 nanoparticles are passed through the microchannel to absorb the heat. The thickness of the solid base remains the same across all configurations, with $t_s = 1mm$. The studied geometries for RRM, OFM, and RROFM designs are presented in Table I. Only one configuration for RRSDM has been studied, denoted as RRSDM-REF, where $Z_u = 500\mu m$. It has the same rib characteristics as design SCM but differs from the other designs by the insertion of a straight fin with $\delta_{f,2} = 100\mu m$ and $L_{f,2} = 4.5mm$, creating a subdivided microchannel at the second length of the microchannel.

The thickness of the solid base remains the same across all configurations, with $t_s = 1mm$. The studied geometries for RRM, OFM, and RROFM designs are presented in Table I. Only one configuration for RRSDM has been studied, denoted as RRSDM-REF, where $Z_u = 500\mu m$. It has the same rib characteristics as design SCM but differs from the other designs by the insertion of a straight fin with $\delta_{f,2} = 100\mu m$ and $L_{f,2} = 4.5mm$, creating a subdivided microchannel at the second length of the microchannel.

III. Numerical Methods

The computational fluid dynamics ANSYS Fluent software was employed for solving the steady states simulations under the following assumptions:

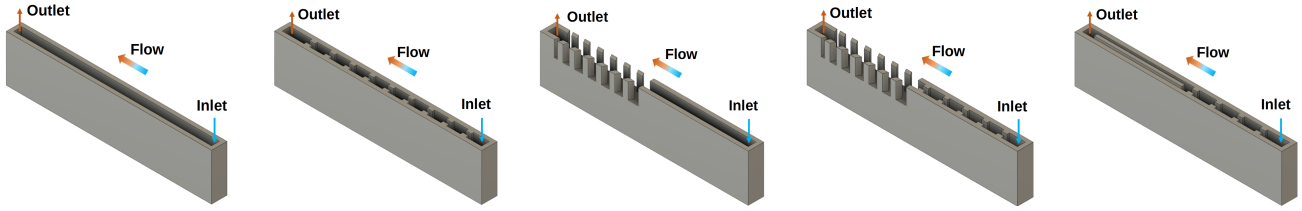

(a) SCM (b) RRM (c) OFM (d) RROFM (e) RRSDM

Fig. 3: Schematic diagram of the studied microchannel heat sink designs in the present work, (a) conventional smooth straight microchannel, (b) design with rectangular ribs only, (c) design with oblique fins only, (d) design combining rectangular ribs and oblique fins, (e) design with ribs and subdivided microchannel.

TABLE I: Geometrical properties of the studied configurations for designs RRM, OFM, and RROFM

Design RRM		**Design OFM**		**Design RROFM**	
configuration	parameters	configuration	parameters	configuration	parameters
RRM-REF	$Z_u = 500\mu m$, $N_r = 9$ $P_r = 900\mu m$, $L_r = 200\mu m$	OFM-REF	$Z_u = 500\mu m$, $\beta = 60°$, $L_f = 200\mu m$	RROFM-REF	$Z_u = 500\mu m$, $L_r = 200\mu m$, $e_r = 80\mu m$ $N_r = 4$
RRM-P080 RRM-N5	$P_r = 800\mu m$ $N_r = 5$	OFM-D300 OFM-D400 OFM-D600 OFM-E70 OFM-E90 OFM-L150 OFM-L300 OFM-L350	$Z_u = 300\mu m$ $Z_u = 400\mu m$ $Z_u = 600\mu m$ $e_r = 70\mu m$ $e_r = 90\mu m$ $L_r = 150\ \mu m$ $L_r = 300\mu m$ $L_r = 350\mu m$	RROFM-D300 RROFM-D400 RROFM-D600 RROFM-A50 RROFM-A70 RROFM-L250 RROFM-L300 RROFM-L350	$Z_u = 300\mu m$ $Z_u = 400\mu m$ $Z_u = 600\mu m$ $\beta = 50°$ $\beta = 70°$ $L_f = 250\mu m$ $L_f = 300\mu m$ $L_f = 350\mu m$

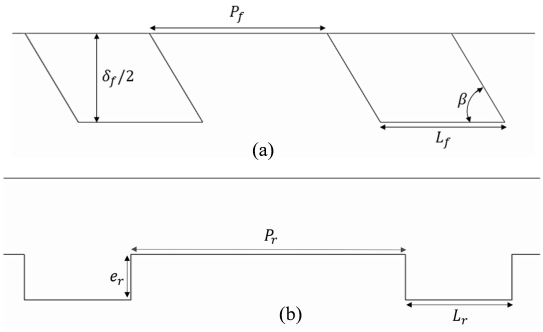

Fig. 4: (a) Oblique fins relative geometrical quantities, P_f is the fins pitch, L_f the fin length and β the oblique fin angle. (b) Ribs geometrical quantities, P_r is the ribs pitch, L_r the rib length and e_r the rib height.

- Heat transfer and fluid flow are steady.
- The fluid flow is single phase, continuous, incompressible, laminar ($Re \in [150, 900]$), and three-dimensional.
- The temperature-dependent thermal physical properties of the working fluid and the solid are constant.
- External heat transfer phenomena between the outer walls are not taken into consideration except for the heated base wall.
- Viscous heating in neglected as the Brinkman number, $Br = \frac{\mu U^2}{k_s \Delta T}$, remains lower than unity.

A. *Boundary conditions*

The following boundary conditions for the solid and fluid systems are imposed in the numerical model.

- Inlet: uniform velocity of coolant with constant temperature $T_{in} = 293K$ is applied.
- Outlet: Zero pressure outlet condition is applied.
- Fluid/Solid interface: no-slip boundary condition, heat flux, and temperature continuity are satisfied.
- Heated wall: a constant heat flux is applied $-k_s \frac{\partial T_s}{\partial n} = q_b = 100W/cm^2$.
- Other solid walls: these walls are set to be adiabatic.

B. *Nanofluid homogeneous model*

In this work, a homogeneous nanofluid model is used to simulate Al_2O_3 nanoparticles mixed with water at four different volume fraction concentrations $\{1\%, 2\%, 3\%, 4\%\}$. This model considers an equivalent single-phase liquid in the numerical simulation, referred to as nanofluid. The thermal physical properties of the nanofluid are computed from [14].

C. *Grid independence test*

It is imperative to verify that the meshing grid does not affect the outcome. Therefore, three different mesh element sizes, using the tetrahedral meshing method and refinement near the obstacle edges, were tested and compared for a median Reynolds number value. The results are given in Table. II and show only slight variations of the output parameters for

TABLE II: Grid independence test for design RRM.

Element size (μm)	Number of elements (-)	T_{max} (K)	ΔP (kPa)	Relative error (%)
40	73588	332.82	0.461	3.79
50	44059	332.92	0.434	2.35
60	36519	332.04	0.439	1.23
Mean value		332.59	0.444	

the different mesh sizes. The computed error is relative to the mean value of the three outputs.

IV. Results and Discussions

Nanoparticles volume fraction: In Fig. 5(a), we observe a decrease in the average temperature of the heated wall as the nanoparticle volume fraction increases. This decline is primarily attributed to the enhancement of the convective heat exchange coefficient, as depicted in Fig. 5(b), owing to the heightened thermal conductivity and density of the coolant. Additionally, we note an increase in the convective heat transfer coefficient with a rising Reynolds number. This phenomenon is attributed to developing flow effects, particularly the emergence of thermal and dynamic boundary layers away from the inlet as velocity increases. Consequently, more heat is absorbed, and the coolant outlet temperature also rises with nanoparticle volume fraction.

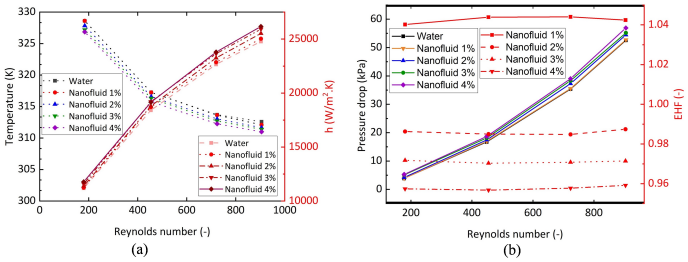

Fig. 5: Nanoparticle volume fraction performance analysis diagrams: (a) average heated wall temperature and convective heat exchange coefficient, (b) total pressure drop, and enhancement factor.

Conversely, the pressure drop is also an increasing function of the nanoparticle volume fraction, as shown in Fig. 5(a). This slight augmentation is mainly due to the increased value of dynamic viscosity and density. However, it is necessary to note that this pressure drop will be even higher due to nanoparticle deposition and Brownian motion, which are not taken into account in the homogeneous model. Finally, the parabolic law of pressure drop as a function of fluid velocity, and therefore of Reynolds number, is also observed. In order to compare global performance, an Enhancement Factor ($EHF = \frac{COP_{nf}}{COP_w}$) regarding the working fluid has been introduced. The proposed coefficient of performance (COP), which accounts for both hydraulic and thermal performance effects, is as follows.

$$COP_f = \frac{\dot{Q}_{heat}}{\dot{W}_{pump}} = \frac{\dot{m} C_{p,f} \Delta T_f}{\dot{V} \Delta p} \quad (1)$$

Results in Fig. 5(b) show a slight enhancement for $\phi = 1\%$. However, for other volume fractions, the increase in pressure drop outweighs the thermal improvement, resulting in lower overall performance. This figure also highlights the limitations of the homogeneous nanofluid model, as it suggests no variation of the Enhancement Factor (EHF) with respect to the Reynolds number. The model does not account for the effect of velocity on the motion of nanoparticles. In the next analysis, only water will be used as a coolant, and similar trends to those observed in this section can be expected for each of the subsequent studies.

Microchannel depth: In this section, we study the effects of varying the microchannel depth while maintaining a constant solid wall thickness of 1 mm, using water as the working fluid and a fixed Reynolds number. We investigate designs OFM and RROFM (Fig. 6), with corresponding configurations (Table I): OFM-REF, OFM-D300, OFM-D400, OFM-D600, RROFM-REF, RROFM-D300, RROFM-D400, RROFM-D600. Increasing the microchannel depth weakens the mechanical structure and stability of the fins. Ribs have been added to design RROFM to address this issue. Deeper microchannels result in lower average temperature of the heated wall and thermal resistance for both designs. Design RROFM performs better, as seen in Fig. 6, attributed to the increased heat exchange area with deeper microchannels. However, ribs induce a higher pressure drop. Additionally, the convective heat exchange coefficient decreases with depth, consistent with the hydraulic diameter increase. Fig. 6 shows that, for a given pump power, deeper microchannels achieve lower heated wall temperatures.

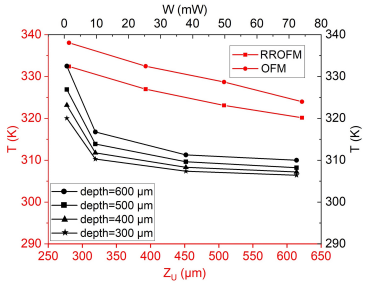

Fig. 6: Performance analysis for different microchannel depths: deeper channels offer better thermal performance at fixed pump power due to larger heat transfer area and lower pressure drop from increased hydraulic diameter.

Oblique fin angle and length: Three different angles were implemented: 50°, 60°, and 70°, corresponding to configurations OFM-A50, OFM-REF, and OFM-A70, respectively. The results show no significant difference in both thermal and hydraulic performance. However, the pressure drop evolution reveals that for higher Reynolds numbers and larger angles (Fig. 7(a)), the pressure drop is lower. Square-shaped oblique fins contribute to reduced fluid layer detachment, as indicated

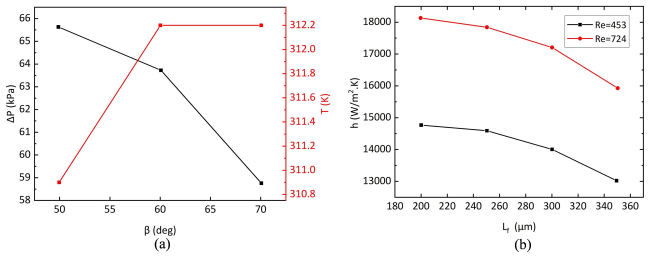

Fig. 7: Performance analysis of microchannel oblique fins with the OFM design includes: (a) the effect of fin angle β on heated wall average temperature and pressure drop at Re=901, and (b) the impact of fin length L_f on the convective heat exchange coefficient at Re=453.

by the slightly higher heated wall temperature. Consequently, a smaller pressure drop implies less disruption and mixing, resulting in less heat transfer enhancement. The determining parameter for choosing the oblique fin angle will be the feasibility of such structures using Additive Manufacturing, with square-shaped fins being easier to manufacture. Such structures have also been studied and manufactured in Collins' paper [16]. Varying the length of the oblique fins, which entails a reduction in the fins' pitch, does not significantly influence the pressure and temperature parameters. Moreover, no clear pattern or conclusion can be drawn on the trend. However, a decreasing trend is observed in the evolution of the convective heat exchange coefficient for all Reynolds numbers (an example for Re = 453 is shown in Fig. 7(b)).

Ribs pitch: For investigating the effects of ribs on thermal and hydraulic performance, we focus on design RRM with its different configurations. Two pitches are implemented (Fig. 8(a)). The temperature profiles show that, for a given pump power, the average temperature of the heated wall is lower with more spaced ribs, particularly pronounced for higher flow rates. Conversely, the convective heat exchange coefficient is higher with smaller ribs' pitch due to better development of boundary layers, aiding heat exchange.

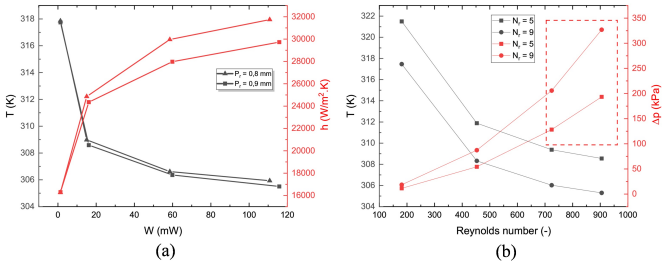

Fig. 8: Ribs pitch and number performance analysis: (a) heated wall average temperature and convective heat exchange coefficient, (b) heated wall average temperature and total pressure drop for two different numbers of ribs.

Ribs number: Reducing the number of ribs, as shown in Fig. 8(b), induces less pressure drop but higher heated wall temperatures due to less thermal boundary layer disruption

TABLE III: Contraction coefficient for cross-section ratios

S_2/S_1	0.1	0.2	0.3	0.4	0.5	0.6
C_c	0.624	0.632	0.643	0.659	0.681	0.712

and mixing effects. However, these results enable us to see that for RRM design, tremendous pressure losses are observed for Reynolds numbers greaterr than 450, indicated by the red-framed area in the figure, which is not suitable for MCHS. This confirms that the reduction of flow length, either by inserting oblique fins, interrupting the flow periodically, or having a manifold with several inlets and outlets as proposed in [17], enables a significant reduction in pressure drop.

Ribs height and length: In this section, the effects of the height of the ribs e_r and the length L_r are analyzed. Similar trends are observed for these two parameters, and the coefficient of performance are plotted in Fig. 9. Therefore, having higher or longer ribs enhances heat transfer and provides lower wall temperatures despite higher pressure drops. In fact, higher ribs increase the heat transfer area but also disrupt the thermal boundary layer. On the other hand, the resulting constriction increases both regular and singular pressure losses due to the working fluid flowing through a smaller channel and larger cross-sectional ratio. If we denote S_1 and S_2 as the larger and smaller cross sections respectively, the singular pressure drop coefficient for both entering and exiting the shrunken channel is $K_{in} = \left(\frac{1}{C_c} - 1\right)^2$, and $K_{out} = \left(1 - \frac{S_2}{S_1}\right)^2$ [18]. where C_c is an increasing function of the ratio S_2/S_1 as given in table III. COP for both parameters is decreasing for bigger heights and lengths due essentially to higher pressure drop.

Designs comparison: In this section, we compare the four designs studied. The RRSDM design consists of subdividing the second part of the microchannel into two smaller microchannels separated by a straight rectangular fin ($\delta_{f,2} \times L_{f,2}$). This subdivision reduces the hydraulic diameter and thus increases the convective heat exchange in this region while also disrupting thermal boundary layers. The performance of the designs was compared for the same geometric quantities, that is, the same microchannel depth ($Z_u = 500\mu m$) and microchannel width. For the oblique fins and ribs, the reference configurations were taken. Results in Fig. 10 show that microchannels with continuous walls, i.e., design

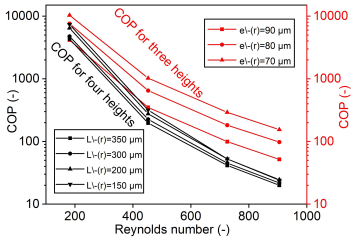

Fig. 9: Effect of rib height and length: both reduce global performance as they increase pressure drop, but rib height has a greater impact than rib length.

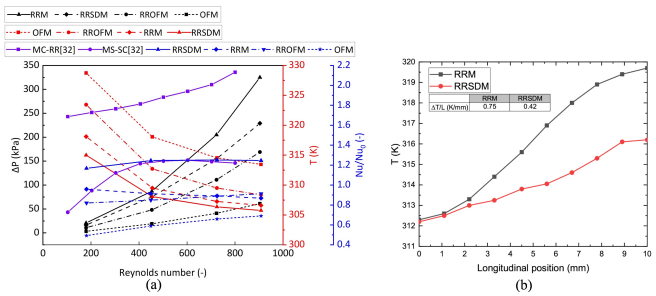

Fig. 10: Performance comparison of the studied designs: (a) total pressure drop vs. Reynolds number, heated wall average temperature, and temperature gradient at Re = 181, (b) global performance for smooth and conventional microchannels.

RRM and design RRSDM, have much higher pressure drop even though they provide lower heated wall temperature. The overall total resistance for each design and other values from literature are also reported for comparison purposes in Table IV.

TABLE IV: Performance comparison with other MCHS

Study	Reynolds number	Δp (kPa)	R_{tot} (K/W)
RRM	475	20	0,245
OFM	255	20	0,336
RROFM	250	35	0,251
RRSDM	275	35	0,211
SMC [16]	1060	20	0,305
MMC [16]	1180	15	0,485

In Fig. 10, we compare the performance of different designs. Fig. 10(a) displays the pressure drop and average wall temperature evolution with Reynolds numbers. The RRSDM design achieves the lowest wall temperature without the highest pressure drop. This design also exhibits superior thermal performance and temperature uniformity, as confirmed in Fig. 10(a). The smaller channels at the end of the second microchannel part enhance heat transfer by increasing convective effects. Furthermore, we evaluate global performance compared to other designs in the literature [11], [19]. The RRSDM design falls within the heat enhancement range, while the OFM design shows lower performance due to a smaller PEC, attributed to fluid stagnation between oblique fins. A design with periodically interrupted oblique fins, as proposed in [7], could address this limitation.

V. Conclusion

In this study, four unique designs for MCHS utilizing geometric structures and additive fluids to enhance overall performance were investigated. It has been demonstrated that introducing oblique fins or periodically separated microstructures can reduce pressure drop, with these structures being suitable for Additive Manufacturing. Additionally, deeper microchannels have been shown to improve both thermal and hydraulic performance. However, deeper microchannels may compromise the mechanical structure, particularly for isolated fins or shapes as studied here. Thus, finding a compromise between thermal dissipation, pressure drop, and structural stability is essential. This research has provided insights into the influence of different geometric parameters on the overall performance of the four new MCHS designs. The fourth design model achieved an average temperature of 41°C under a total pressure drop of $\Delta p = 18.57$ kPa. Future line of work involves experimental validation of the proposed designs using additive manufacturing.

References

[1] B. K. Bose, "Power semiconductor devices," Power Electronics and Motor Drives, second edition, 2021.

[2] R. Parida et al., "Multi-layer mini-channel and ribbed mini-channel based high-performance cooling configurations for automotive inverters—part a: Design and evaluation," Journal of Thermal Science and Engineering Applications, vol. 5, no. 3, 2013.

[3] D. B. Tuckerman and R. F. W. Pease, "High-performance heat sinking for vlsi," IEEE Electron device letters, vol. 2, no. 5, pp. 126–129, 1981.

[4] W. Japar et al., "A review of passive methods in microchannel heat sink application through advanced geometric structure and nanofluids: Current advance- ments and challenges," Nanotechnology Reviews, vol. 9, no. 1, 2020.

[5] M. Hajmohammadi et al., "Effects of applying uniform and non-uniform external magnetic fields on the optimal design of microchannel heat sinks," Int. Journal of Mechanical Sciences, vol. 186, 2020.

[6] L. Léal et al., "An overview of heat transfer enhancement methods and new perspectives: Focus on active methods using electro-active materials," Int. Journal of Heat and Mass Transfer, vol. 61, 2013.

[7] Z. Feng et al., "Effects of geometric parameters of circular pin-fins on fluid flow and heat transfer in an interrupted microchannel heat sink," International Journal of Thermal Sciences, vol. 165, p. 106956, 2021.

[8] A. Rajalingam and S. Chakraborty, "Effect of shape and arrangement of micro-structures in a microchannel heat sink on the thermo-hydraulic performance," Applied Thermal Engineering, vol. 190, p. 116755, 2021.

[9] Y. Yan et al., "Single/multi-objective optimizations on hydraulic and thermal management in micro-channel heat sink with bionic y-shaped fractal network by genetic algorithm coupled with numerical simulation," International Jour- nal of Heat and Mass Transfer, vol. 129, 2019.

[10] G. Criscuolo et al., "Experimental characterization of the heat transfer in multi-microchannel heat sinks for two- phase cooling of power electronics," Fluids, vol. 6, no. 2, p. 55, 2021.

[11] I. A. Ghani et al., "Heat transfer enhancement in microchannel heat sink using hybrid technique of ribs and secondary channels," Inter- national Journal of Heat and Mass Transfer, vol. 114, pp. 640–655, 2017.

[12] R. Vinoth and B. Sachuthananthan, "Flow and heat trans- fer behavior of hybrid nanofluid through microchannel with two different channels," Int. Communica- tions in Heat and Mass Transfer, vol. 123, 2021.

[13] M. Sarafraz et al., "Thermal performance of a heat sink microchannel work- ing with biologically produced silver-water nanofluid: experimental assessment," Experimental Thermal and Fluid Science, vol. 91, pp. 509–519, 2018.

[14] M. Xuan and W. Roetzel, "Conceptions for heat transfer correlation of nanofluids," International Journal of heat and Mass transfer, vol. 43, no. 19, pp. 3701–3707, 2000.

[15] K. Yu et al., "Cfd analysis of nanofluid forced convection heat transport in laminar flow through a compact pipe," in Journal of Physics: Conference Series, vol. 885. IOP Publishing, 2017, p. 012021.

[16] L. Collins et al., "Evaluation of additively manufactured microchannel heat sinks," IEEE Transactions on Components, Pack- aging and Manufacturing Technology, vol. 9, no. 3, pp. 446–457, 2018.

[17] W. Escher et al., "Experi- mental investigation of an ultrathin manifold microchan- nel heat sink for liquid-cooled chips," Journal of Heat Transfer, vol. 132, 2010.

[18] A. LALLEMAND, "Fluidflow, flow in pipes, networks," Techniques de l'Ingénieur, vol. 1, no. BE8161, 2001.

[19] I. A. Ghani et al., "Heat transfer augmentation in a microchannel heat sink with sinusoidal cavities and rectangular ribs," Interna- tional Journal of Heat and Mass Transfer, vol. 108, pp. 1969–1981, 2017.